

Characterization of Hydraulically Induced Fracture in Lab-scale Enhanced Geothermal Reservoir

Lianbo Hu, Ahmad Ghassemi

**Reservoir Geomechanics and Seismicity Research Group, The University of Oklahoma,
Norman, OK, USA**

John Pritchett, Sabodh Garg

Leidos Inc, San Diego, CA, USA

Keywords

Enhanced geothermal system, Laboratory scale, Self-potential, Acoustic emission, Hydraulic fracturing, Circulation, Tracers

ABSTRACT

Geothermal energy production by water circulation in man-made fracture systems is referred to as enhanced or engineered geothermal systems (EGS) production. The fluid/heat flow properties of the induced fracture are essential for predicting later geothermal development. In this work, we study the creation and characterization of hydraulically induced fracture on a laboratory scale using acoustic emission (AE) cloud, spontaneous potential (SP), and tracer analysis. To achieve this goal, we have performed reservoir stimulation using 13x13x13 inch³ cubical rock samples under representative in-situ stress regimes. During this stimulation stage and the subsequent production processes, sensors are used on the block surfaces and within cavities and wellbores to characterize and locate acoustic emissions (AE) caused by the stimulation, and to monitor local changes in fluid pressure, temperature, and electrical self-potential (SP). Cold water is injected centrally and simultaneously collected from nearby miniature production wells. Water with tracer was injected after the circulation test, and concentrations in fluid collected from the production wells could be measured. The data collected could be then analyzed to develop a better understanding of the fractures and the induced fracture permeability and fluid/heat flow.

1. Introduction

Geothermal energy is considered to be a promising option for a future clean and sustainable energy supply. However, certain technical barriers need to be removed for large scale utilization of the resources. Particularly, questions related to reservoir creation in different rock types and stress conditions need be addressed, and good characterization of the induced or

activated fracture will then provide fundamental information needed to evaluate and then develop the enhanced geothermal system. Laboratory scale studies present a good opportunity to help resolve some of the pending challenges along with recent field-scale efforts within the framework of the FORGE (Frontier Observatory for Research in Geothermal Energy) initiative. The main purpose of this project is to gain a better understanding of the geometry and the heat exchange properties of the hydraulically induced fractures in enhanced or engineered geothermal systems (EGS). To realize this goal, a new lab-scale hydraulic fracture test system has been developed that allows us to replicate aspects of the EGS hydraulic fracturing treatment in the field. Our work improves the state-of-the-art by allowing the simultaneous monitoring of acoustic emission (AE), spontaneous potential (SP) and tracers during the stimulation and circulation phases. In this work, our most recent promising result will be presented and discussed.

2. The Lab-Scale EGS Test System

The lab-scale EGS system has several integrated subsystems. The main subsystems are: a polyaxial frame and heaters, hydraulic fracturing and circulation systems, temperature, AE and SP data acquisition systems, and fluids and tracers. Figure. 1 (left) shows the fully assembled test systems. Sensors on the block surfaces and within cavities and wellbores allow us to characterize and locate AE caused by the stimulation and to monitor local changes in fluid pressure, temperature, and SP. The polyaxial frame can be sealed with high pore pressure in the test block and may be pre-heated to simulate a geothermal system. Multiple wells can be drilled into the test block to simulate injection and production. Fluid produced from the production wells can be collected and analyzed. Figure.1 (right) shows a granite block to be tested with sensors and hydraulic tubing. More information about these subsystems is provided by Hu (2016).

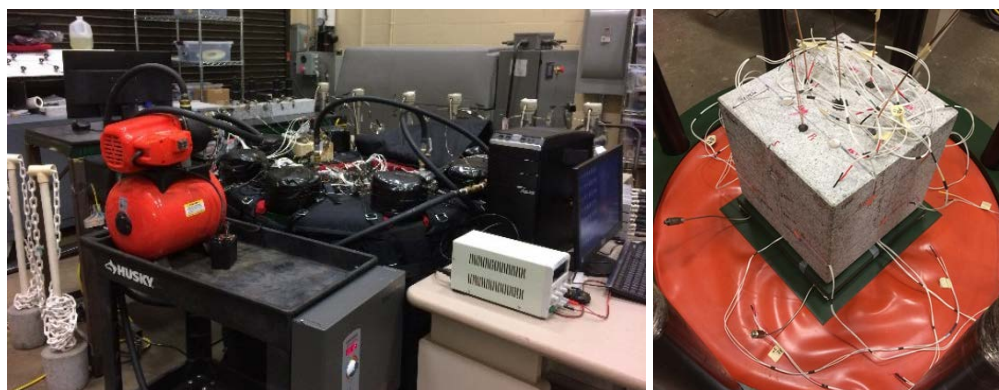


Figure 1: Fully assembled test system and granite block to be tested.

3. Laboratory Test Result

3.1 Test Setup

In this section, some promising test results from a 13.0 inch cubical Sierra White granite block will be presented and discussed. Figure. 2 (left) is a top view showing the layout of the wells and the AE sensors on the top surface, and Figure. 2 (right) is a longitudinal sectional view of the sample showing the interior layout of the wells. The injection hole was drilled with a 0.75 inch diameter drill bit from the center of the top surface. The injection well has a drilled depth of 7.5

inch and a diameter of 0.79 inch. High strength epoxy was poured into the hole to seal the annulus between the injection tubing and the wellbore wall, leaving a 2.0 inch unsealed injection interval at the bottom. Four production wells with depths of 9.0 inch were drilled 3.5 inches away from the injection well and have 5.0 inch unsealed production intervals at the bottom. The diameter of the production wells is 0.39 inch. A thermistor was located at the center of each downhole unsealed interval to measure temperature histories. SP sensors were placed in each well, and the one in the injection well served as the reference electrode. The SP sensors were made by soldering a copper cable to a thin circular copper sheet. Epoxy cylinders with diameter slightly smaller than the wellbores were put inside the wells to occupy space and thus to minimize the effect of wellbore storage. The locations of SP sensors and AE sensors are shown in Figure. 3. The space between the rock block and the inner surface of the loading frame is occupied by flatjacks, PEEK plates and steel plate spacers. After the sample was put into the frame and the frame was fully assembled, principal stresses were applied by injecting oil into the flatjacks to predetermined pressure levels. To prevent the induced fracture from reaching the block boundaries, the hydraulic fracturing process was conducted carefully by monitoring the AE record and the pressure variations in the production wells and careful control of the injection rate.

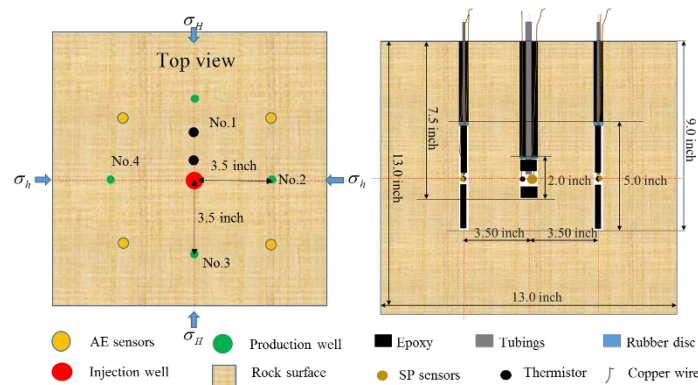


Figure 2: Layout of injection well (left) and production wells with sensors (right).

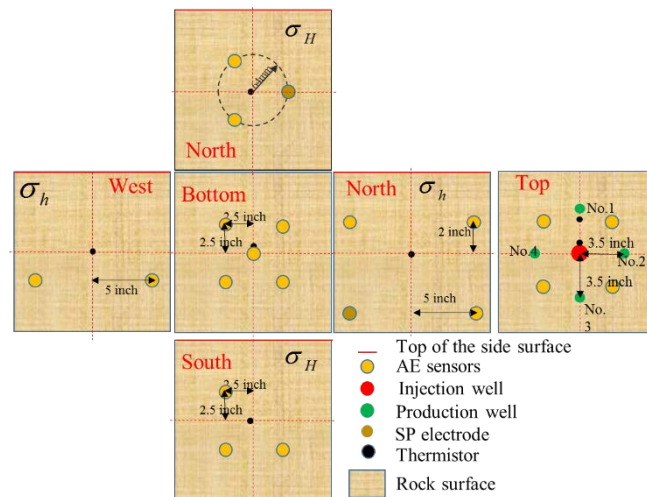


Figure 3: Fold-out diagram of the Sierra White block with AE sensors and SP sensors.

3.2 Test Parameters and Results of the Fracturing Test

The hydraulic fracturing test was conducted without fluid in the frame using the stress conditions listed in Table 1. To enable SP measurements, we saturated the inner part of the block in the vicinity of the wells by maintaining the pressure in the injection and production wells at 250 psi and 100 psi, respectively over forty hours. Totally, about 186 ml 0.002 mole/L NaCl was injected. The total pore volume of the block is about 288 ml calculated from its porosity. For better control of the fracture propagation, the initial injection rate was set to be 2.0 ml/min. The hydraulic fracturing test was conducted at room temperature.

Table 1: Experimental parameters for Sierra White granite block

σ_v , psi	σ_h , psi	σ_H , psi
500	1000	1500

As mentioned above, the hydraulic fracturing phase was carefully conducted. The injection pump was programmed to go into backflow mode or to reduce the injection pressure when the injection pressure drop exceeded a preset value of 40 psi. During the first, second and fourth injection cycles, the pump did backflow and it stopped pumping during the third circle when the pressure drop exceeded higher than 40 psi. At the beginning of the fracturing test, all production wells were closed and if the pressure in the well exceeded 500 psi, the valve for that well was opened. Figure 4 shows the recorded data for the test, namely the injection pressure (dark red), the flow rate (blue), the SP response (purple, pink), and the cumulative AE hits (dark cyan). According to the AE data the main fracture initiation and propagation events occurred during the first and third pressure drop. The maximum pressure difference between the second and fourth injection cycle is 1560 psi (=2991 psi- 1430 psi), which is very close to the rock tensile strength (1549 psi from the Brazilian test).

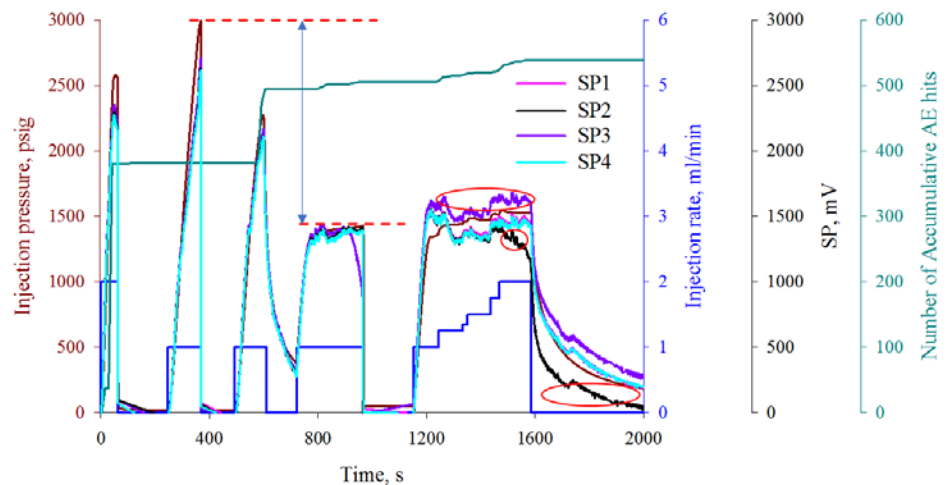


Figure 4: The recording data for Sierra White granite block test.

The SP response indicates that Well No.2 and Well No.3 were intersected by the induced fracture. There is an apparent difference in the SP response of different production wells during the last period of injection. SP1 and SP4 overlap each other, however, SP3 is higher. This is

because the electrokinetic coupling coefficient from injection well to Well No.3 is higher due to the fracture (note that Well 3 valve is open and the pressure in Well 1 and Well 4 is close to 0 psi, so the pressure difference was almost same in these three wells). In Well 2, the pressure increased due to the hydraulic fracture, so the SP2 is the lowest.

To provide a better understanding of the relationship between the pressure difference (the difference in pressure in the injection well and the production well) and the SP recording, a plot of pressure difference vs SP3 is shown in Figure 5. Excellent proportionality is observed between the pressure drop and SP response at difference time intervals: before (0-965 s) and after (1150-1212s) hydraulic fracturing. The electrokinetic coupling coefficient is defined as the ratio of the SP to the pressure difference (Jouniaux and Pozzi, 1995). For the time interval before fracture, the electrokinetic coupling coefficient is 0.96 mV/psi and it increased to 1.26 mV/psi after fracturing (Figure 5), an increase of about 30.4 %. This increase of electrokinetic coupling coefficient is due to the increased permeability at higher pore pressure in response to dilatancy (microcracks) and the related decreased hydraulic tortuosity, as well as due to increase of zeta potential of the new fracture surface areas.

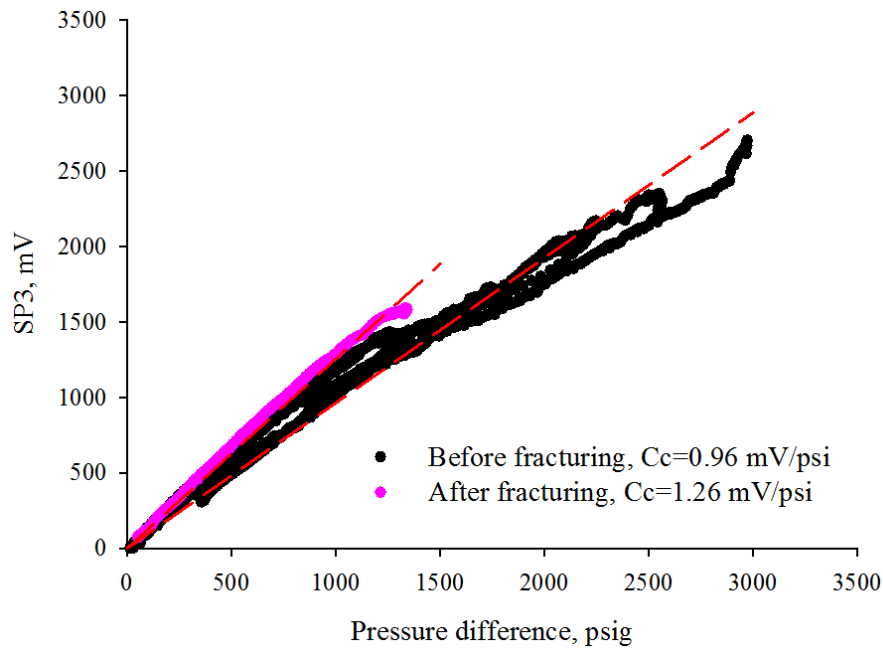


Figure 5: The electrokinetic coupling coefficient for different intervals.

As mentioned before, at the beginning of the fracturing test, all production wells were closed and if the pressure in the well increased to a value higher than 500 psi the valve for that well was opened. The pressure changes in the wells are plotted in Figure 6 indicating which production well was connected with the injection well by the induced hydraulic fracture. In this case, the pressure behavior in the production wells indicates that Well No.2 and Well No.3 were intersected by the fracture after the third injection cycle, and the connection of well No.3 is much stronger than that of Well No.2.

Observation of the fracture after cutting the block shows that the fracture did not reach the rock block surface. However, the fracture created in this test phase of the test was subsequently sealed by the expansion of the rubber disc at the injection well in response to heating (shown in Figure 7) for the circulation phase of the experiment.

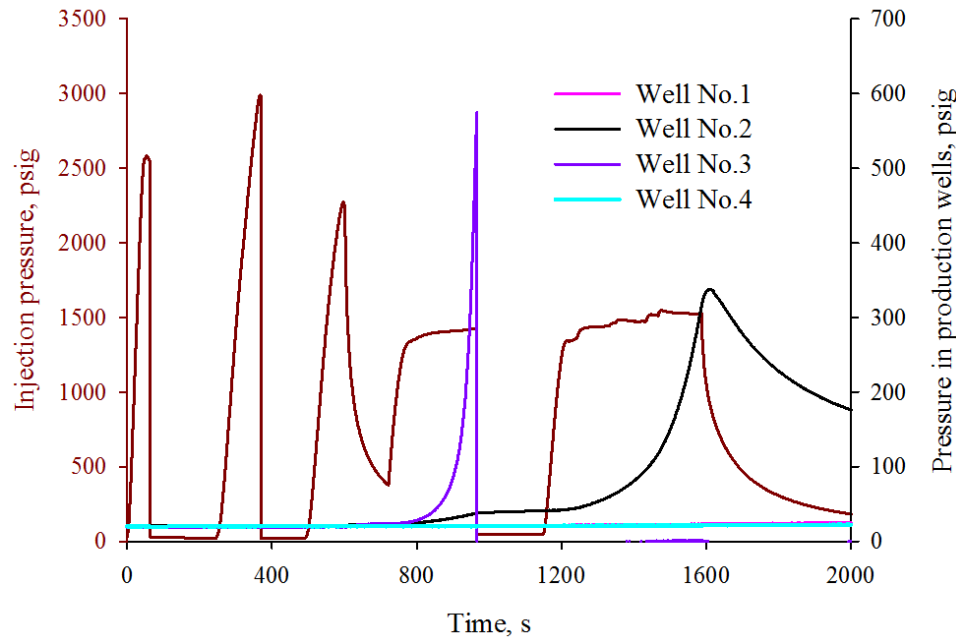


Figure 6: The injection pressure and pressure in production wells.

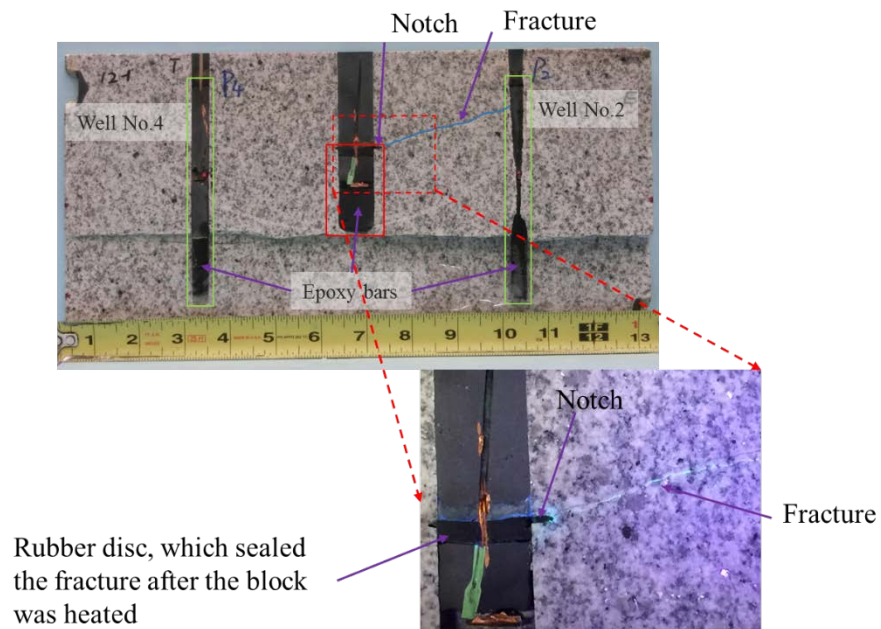


Figure 7: Fracture paths from the injection well.

After hydraulic fracturing, 0.002 mole/L NaCl solution was poured into the loading frame and then the pressure in the loading frame was kept at 50 psi for more than 24 hours to saturate the whole block. After that, a SP measurement was conducted. The purpose of this was to check how the saturation condition would influence the SP response. The SP response in the production wells is plotted in Figure 8. It is obverse that Well No.3 has a slightly higher coupling coefficient due to the fracture. The electrokinetic coupling coefficient was 0.93 mv/psi in Well No.3, which is very close to the value we have before hydraulic fracturing test. This is because the test was conducted with low injection pressure so the fracture was not mechanically opened.

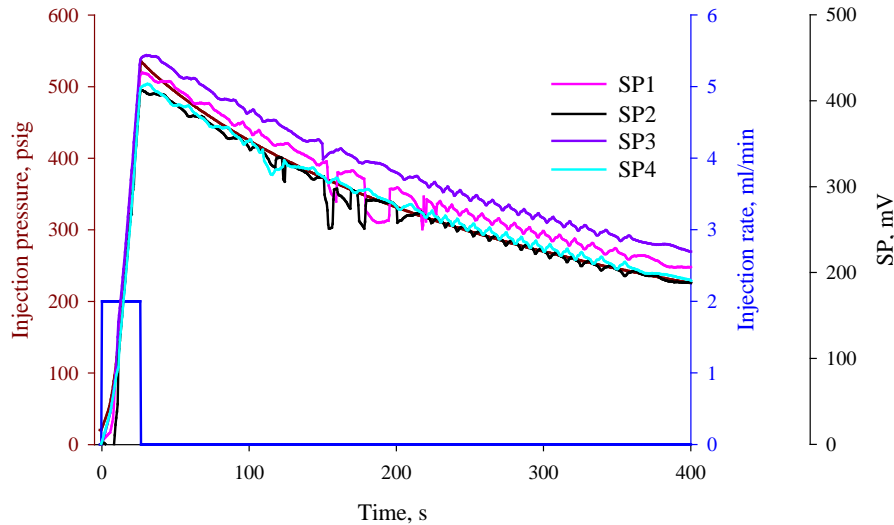


Figure 8: SP check after saturation.

3.4 Circulation Test

3.4.1 New fracture creation

After saturation, the whole block was heated up to a uniform temperature of about 64°C and the same principal stresses were applied. With all the production wells open, cold water was injected at a constant rate of 1.5 ml/min. However, there was no water produced from the production wells No.2 and No.3. This was unexpected since the fracture had connected to well No.2 and No.3 during the hydraulic fracturing phase discussed before. Figure 9 shows the related data in the process. The pumping was stopped when a large pressure drop was detected. The maximum injection pressure was 3841 psi, which was higher than the previous test. Due to the presence of water, the AE noise threshold is high, so only a few AE hits were recorded. The post-fracture observation showed that a new fracture was created during this stage and the previous hydraulic fracture was sealed by the expanded rubber disc.

Figure 10 shows the pressure in all the wells. Although all the production wells were open, we recorded a pressure pulse in Well No.4, which indicates Well No.4 was intersected by the fracture (small pressure rise of 3 psi). We interpret this to mean that the fracture extended to Well No.4.

After the new fracture was created, another injection test was conducted with all production wells shut-in to confirm the connection between injection well and Well No.4. The injection rate was increased from 0.2 ml/min step by step to 2.0 ml/min. When a slight pressure drop was detected and the pressure in Well No.4 raised rapidly, the injection was then ceased. In Figure 11, it is clear that only Well No.4 was connected to the injection well by fracture. Since the fracture created during the first hydraulic fracture test was sealed, no apparent pressure increase in well No.2 and No.3 were detected. Likely, the second fracture was extended from well No.4 a little since a pressure drop was detected.

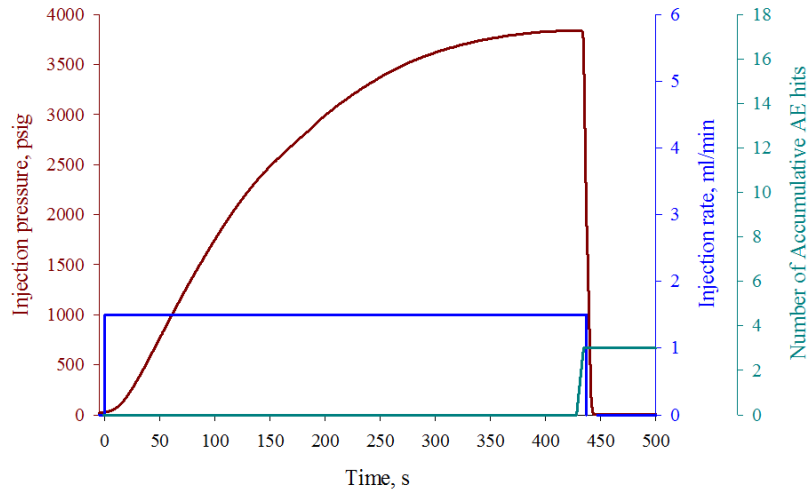


Figure 9: Injection flowrate and pressure, and received cumulative AE hit.

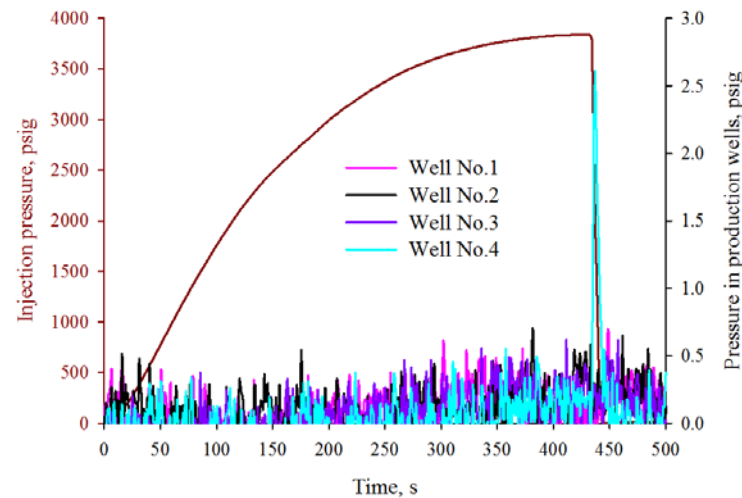


Figure 10: Pressure in wells.

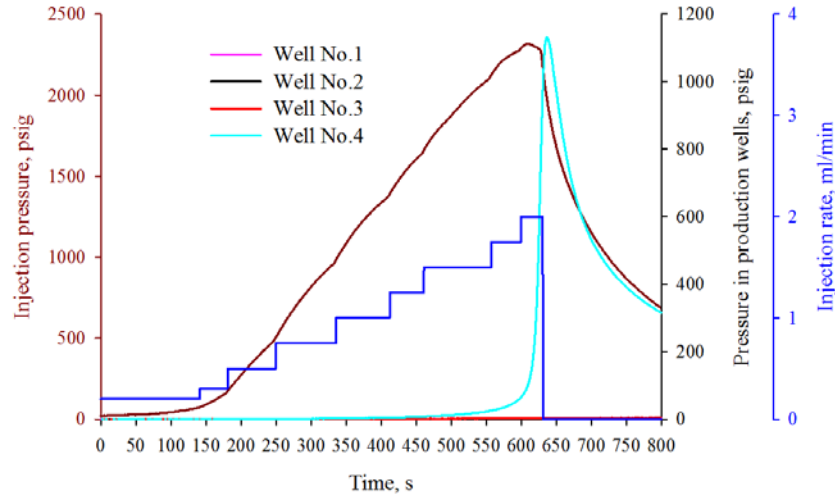


Figure 11: Connection check after well No.4 was intersected.

3.4.2 Circulation through the new fracture

After a good connection between the injection well and production well No.4 was established, a circulation test was conducted using the previous stress level with the initial block temperature of about 63.5°C . During the whole circulation test, all the production well valves were open. Figure 12 shows the injection pressure, injection rate, and the recorded AE hits. To avoid fracture propagation to the rock block surface, the injection rate was slowly increased. The initial injection rate was 1.5ml/min and at the end period of the test, the injection rate was 25.0 ml/min . It can be seen that from Figure 12 the initial injection pressure was high, and it decreased to a constant level at the end of the test. Likely, the fracture slightly extended in another direction away from Well 4 causing the decrease in pressure. The injection pressure was quite high at the beginning after two cycles of low rate injection. The subsequent pressure decrease could result from further fracture propagation and cooling effects.

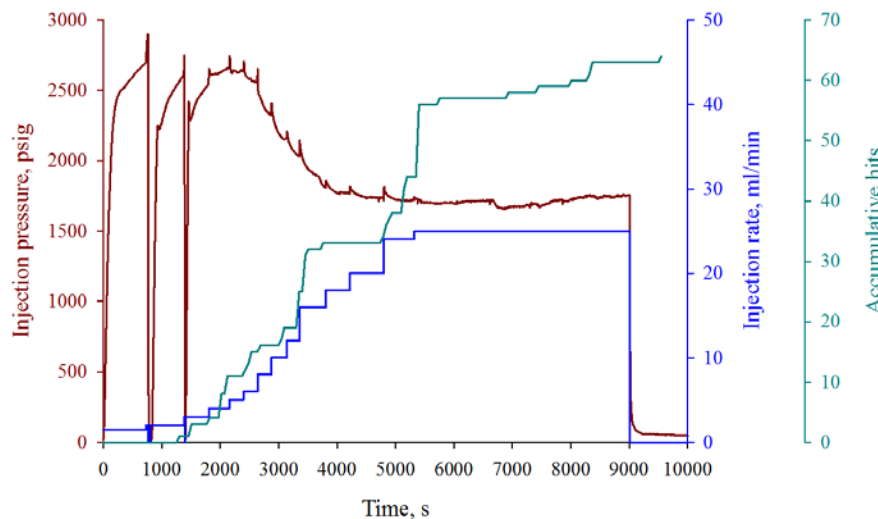


Figure 12: Injection information and the recorded AE during circulation test.

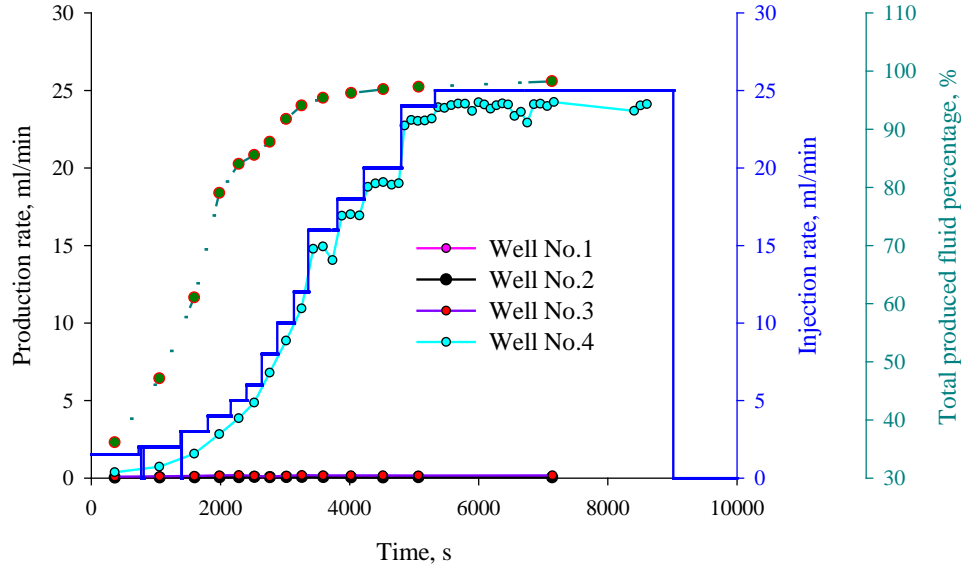


Figure 13: Production information during the circulation test.

During circulation, water produced from the production wells was collected and then weighed to calculate the production rate. Figure 13 shows the injection rate, production rate in wells and the total produced fluid percentage during the circulation test. It indicates that about 95.8% of injection fluid was produced from well No.4 and the flow rate in other production wells were about 2.5% of the injection rate. So, only 1.7% injection fluid was lost to the rock matrix.

The percentage of total produced fluid increases with higher injection rates which is very interesting and useful for field application. If we can avoid extending the fracture too much and also avoid early thermal break through, a higher injection rate could yield a higher water recovery rate and more power supply.

Figure 14 shows the temperature in the wells and the injection rate information during the circulation test. The temperature at the bottom of the injection well decreased with higher injection rate and while the temperature change in the production wells was very small before $t=2840$ s (there are two reasons for this: when the injection rate was low, the injected water was heated up to the block temperature before it reached the bottom of the injection well and also the cooling front had not reached the production wells yet). After a long time of circulation, the well temperatures were: injection well: 20.7°C ; Well No.1: 57.7°C ; Well No.2: 59.3°C ; Well No.3: 57.4°C ; Well No.4: 47.8°C . The temperature drop in these wells are: 43.0°C , 6.1°C , 4.6°C , 6.5°C and 16.0°C , respectively. It is quite clear that since most of the injected water flows to Well No.4, it has highest temperature drop among the production wells. The temperature decrease in other wells was caused by fact that the central part of the granite block was cooled by cold water injection.

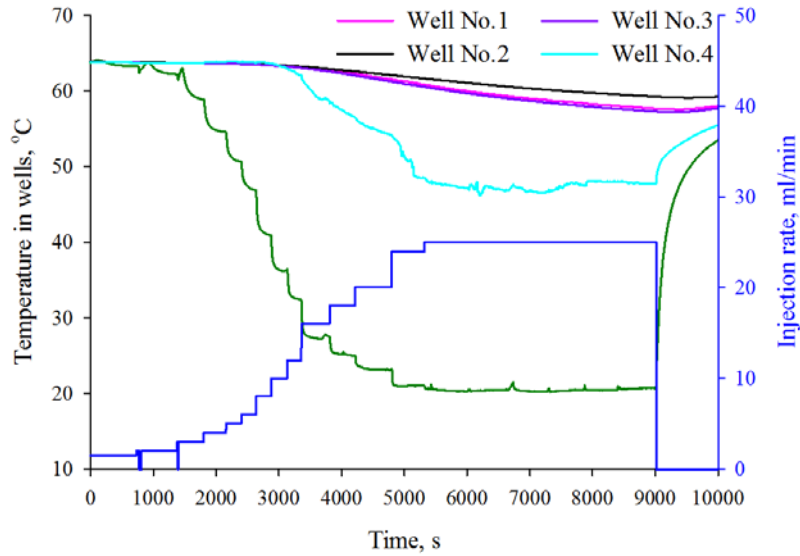


Figure 14: Temperature in the injection well and production wells.

Figure 15 shows the temperature variation on the rock block surfaces. It is apparent that at low injection rate the temperature at the rock surface were almost constant and with higher injection rate the temperature started decreasing further. During the circulation test the temperature drop on the rock surfaces were: top (0, -0.5,13): 6.2°C; top (-2.5,0,13): 2.3°C; west surface: 2.5°C; north surface: 1.6°C; south surface: 1.9°C; east surface: 1.5°C and bottom surface: 2.4°C. The temperature change on the top surface near the injection tubing has the maximum variation (6.2°C). The influence of the injection tubing is limited to a couple of inches around the tubing based on the temperature change of the two points on the top surface.

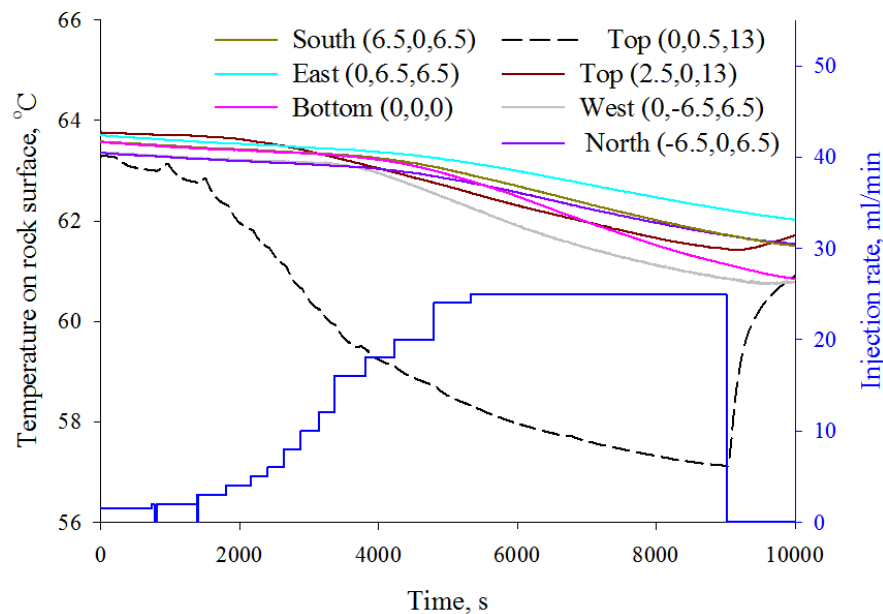


Figure 15: Temperature on the rock surface.

Although it is difficult to determine the fracture fluid/heat flow properties, it is very useful to estimate how much heat was extracted during the circulation test. At first, the water temperature at the injection well head was estimated based on its temperature at the water tank and at the bottom of the injection well. With estimated water temperature at the well head of the production well, the temperature increase was calculated. Note that the injected water is heated not only when flows through the fracture but also when it flows in the wellbore. And due to the block scale in lab, the extracted heat through the wellbore cannot be neglected. Only the flow in Well No.4 is considered because the flow rate in other wells is much smaller. Based on the flowrate and the production temperature the extracted heat was calculated by integrating the heat extraction rate curve from the beginning to the end of the circulation.

Figure 16 shows that a higher injection rate results in a higher heat extraction rate and about 62% of the extracted heat is from the water flowing through the fracture. 421kJ heat was extracted during the circulation stage, with 62 percent (262kJ) of the heat extracted by water flow in the fracture.

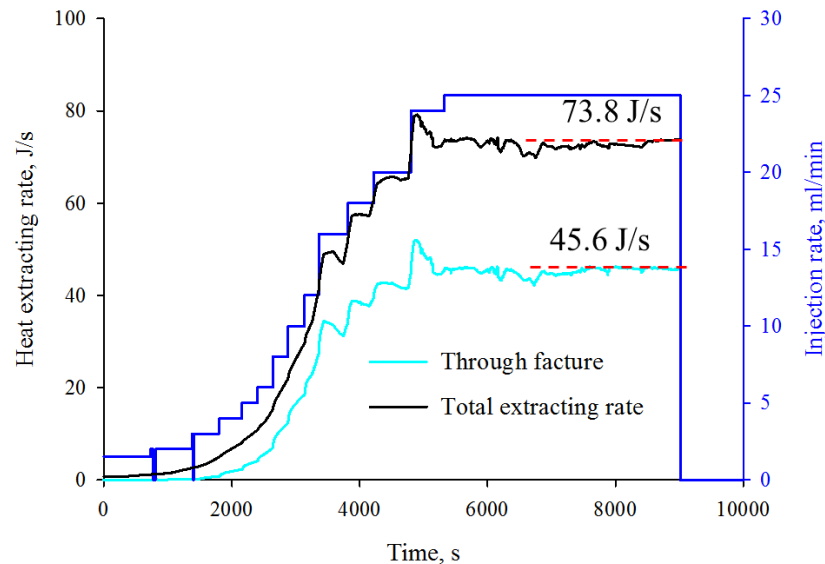


Figure 16: Heat extraction rate from the tested granite block (Mini-EGS).

4. Tracer Test and Fracture Observation

After the circulation test, a tracer test was carried out with the same stress level and temperature was about 62.0°C. As shown in Figure 17, during Phase #1, the injected solution was 1 mole/L NaCl (around 50 times higher than pore fluid) and in Phase #2 the injected solution was 0.02 mole/L NaCl. The injection rate was 1 ml/min. The total injected high concentration fluid is 10.87 ml and the mass of the injected NaCl is 0.64g. Since the production rate was very low and the injected volume of the high concentration fluid is small, the collected fluid from the wells

was diluted and then the conductivity was measured. The concentration of the produced fluid was calculated based on the conductivity of the resulting fluid. Since only Well No.4 was connected to the injection well by induced fracture, the flow rate in Well No.4 was much higher.

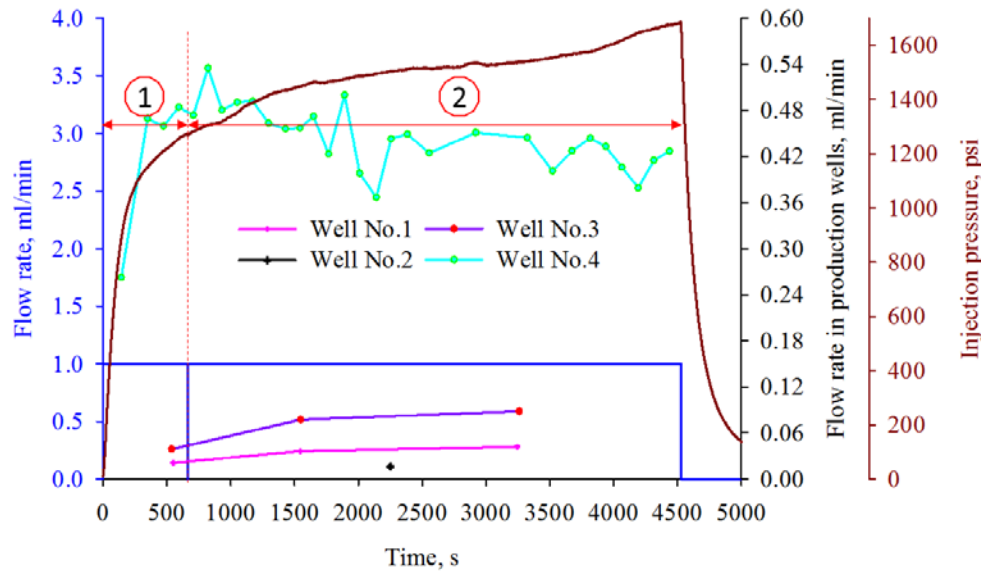


Figure 17: Tracer test information.

The concentration of the fluid was measure and plotted in Figure 18. it reveals that only Well No.4 shows a concentration increase-decrease curve and it is much higher than other wells. There are two apparent linear relationships of trace tail were observed, the first one was dominated by the fracture volume, pipe volume and unoccupied volume in the open interval while the second open interval is due to the matrix leak-off. Some numerical calculation (Tian et al, 2016) also shows this kind of phenomenon. Based on the method of moments, the estimated fracture volume was 0.63 ml.

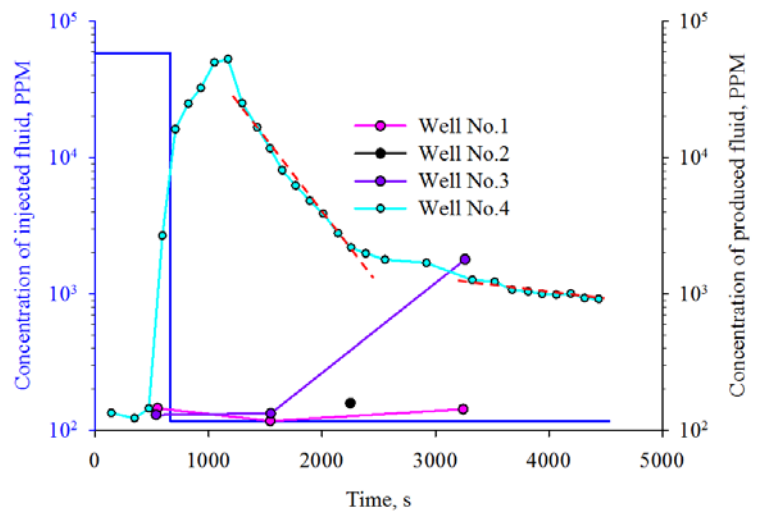


Figure 18: fluid concentration history during the tracer test.

After the test, the granite block was cut into slabs to reveal the fracture trace based on which we can reconstruct the fracture geometry in 3D. Figure 19 (left) shows one of the slab cutting through the injection well. The fracture near well No.4 was emphasized under ultraviolet lamp. The right figure shows the top view of the reconstructed fracture with altitude indicated by color. The fracture initiated at the bottom of the injection well and stopped more than 1.5 inch away from the rock surface and the fracture is a horizontal fracture, the altitude variation is about 0.6 inch. With the fracture area and the fracture volume from tracer test, the calculated fracture width is around 44 μm .

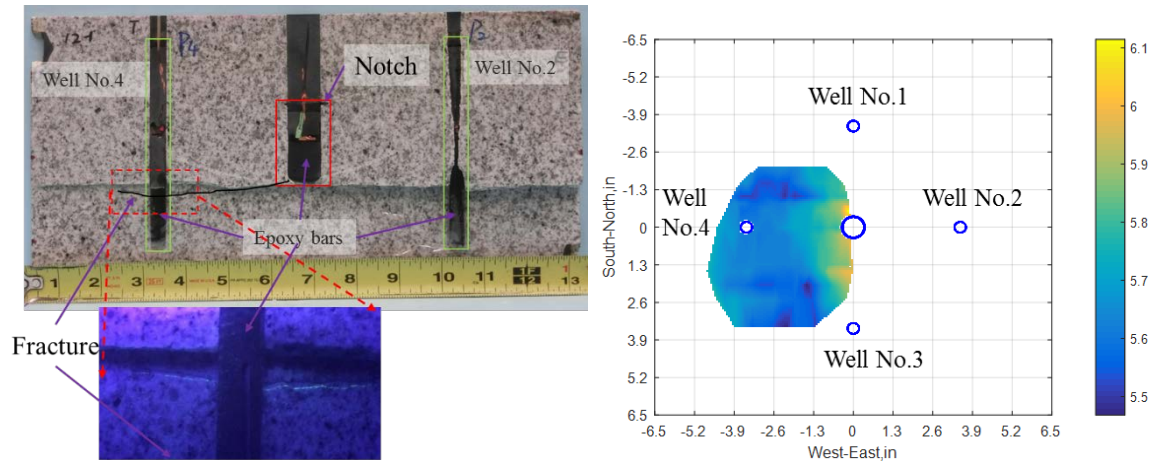


Figure 19: fracture on slab surface (left) and reconstructed fracture (right).

5. Conclusion

We have performed and presented a geothermal reservoir stimulation and production test using $13 \times 13 \times 13$ inch³ pre-heated cubical rock samples under representative in-situ stress regimes. During the stimulation stage, acoustic emissions (AE), pressure and electrical self-potential (SP) were monitored to characterize the induced fracture geometry. Cold water was injected centrally and simultaneously collected from nearby production wells. Temperature in the wells and on the block surfaces was recorded. The maximum temperature drop was as high as 43.0 °C in the injection well and about 16 °C in the production well. The heat extraction analysis shows half of the heat transferred to the injected water was from fracture. A tracer test was carried out after the circulation test without creating new fractures. Tracer test recording shows some result predicted by numerical simulation and the fracture volume was calculated with method of moments. After the fracture geometry reconstruction, the fracture width was estimated to be about 44 μm . Further analysis will be conducted to give more information about the fracture properties such as the permeability and thermal conductivity.

ACKNOWLEDGEMENTS

This project was supported by the U.S. Department of Energy Office of Energy Efficiency and Renewable Energy under Cooperative Agreement DE-EE0006765.0000. This support does not constitute an endorsement by the U.S. Department of Energy of the views expressed in this publication.

REFERENCES

- Fitterman D V. 1978. Electrokinetic and magnetic anomalies associated with dilatant regions in a layered earth. *Journal of Geophysical Research: Solid Earth*. 83(B12): 5923-5928.
- Hubbert, M.K. and Willis, D.G. 1957. Mechanics of Hydraulic Fracturing. *Transactions of AIME*. 153-166.
- Ishido, T., and Pritchett, J. W. 2003. Characterization of fractured reservoirs using continuous self-potential measurements. In *Proc. 28th Workshop on Geothermal Reservoir Engineering*. 158-165
- Ishibashi T, Watanabe N, Hirano N, et al. 2012. Experimental and Numerical Evaluation of Channeling Flow in Fractured Type of Geothermal Reservoir. *Thirty-Seventh Workshop on Geothermal Reservoir Engineering, Stanford University, Stanford, California*.
- Jouniaux L, and Pozzi J P. 1995. Streaming potential and permeability of saturated sandstones under triaxial stress: Consequences for electrotelluric anomalies prior to earthquakes. *Journal of Geophysical Research: Solid Earth*. 100(B6): 10197-10209.
- Morgan, F. D. 1989. Fundamentals of streaming potentials in geophysics: Laboratory methods. In *Detection of subsurface flow phenomena*. Springer Berlin Heidelberg. 133-144
- MIT-Led Report. 2006. *The Future of Geothermal Energy*, ISBN: 0-615-13438-6.
- Pritchett, J. W., and Ishido, T. 2005. Hydrofracture characterization using downhole electrical monitoring. In *Proceedings of World Geothermal Congress, Turkey*.
- Yang Y, Zhang L, Lv J, et al. 2012. Experimental study on fracture process of concrete by acoustic emission technology. *Przegląd Elektrotechniczny*. 88(9b): 55-58.
- Hu L, Ghassemi A, et al. 2016. Laboratory Scale Investigation of Enhanced Geothermal Reservoir Stimulation. *Forty first Workshop on Geothermal Reservoir Engineering, Stanford University, Stanford, California, February 22-24, 2016*
- Tian, W., et al., 2016. Estimation of hydraulic fracture volume utilizing partitioning chemical tracer in shale gas formation, *Journal of Natural Gas Science and Engineering*, <http://dx.doi.org/10.1016/j.jngse.2016.06.018>